



1 **Physicochemical and Temporal Characteristics of Individual**
2 **Atmospheric Aerosol Particles in Urban Seoul during KORUS-AQ**
3 **Campaign: Insights from Single-Particle Analysis**

4

5 Hanjin Yoo^{1,2}, Li Wu³, Hong Geng^{4,+}, and Chul-Un Ro^{1,2,+}

6

7 ¹Department of Chemistry, Inha University, Incheon, 22212, Republic of Korea

8 ²Particle Pollution Management Center, Inha University, Incheon, 21999, Republic of Korea

9 ³School of Earth Science System, Tianjin University, Tianjin, China

10 ⁴Institute of Environmental Science, Shanxi University, Taiyuan, China

11

12 *Correspondence to:* Chul-Un Ro (curo@inha.ac.kr) and Hong Geng (genghong@sxu.edu.cn)

13

14 **ABSTRACT**

15 Single-particle analysis was conducted to characterize atmospheric aerosol particles
16 collected at Olympic Park in Seoul, Korea as a part of the KORUS-AQ campaign which was
17 carried out during May-June 2016. The KORUS-AQ campaign aimed to understand the
18 temporal and spatial characteristics of atmospheric pollution on the Korean Peninsula through
19 an international cooperative field study. A total of 8004 individual particles from 52 samples
20 collected between 5/23-6/5, 2016, were investigated using a quantitative electron probe X-ray
21 microanalysis (low-Z particle EPMA), resulting in the identification of seven major particle
22 types. These included genuine and reacted mineral dust, sea-spray aerosols, secondary aerosol
23 particles, heavy metal-containing particles, combustion particles, Fe-rich particles, and others
24 (biogenic and humic-like substances (HULIS) particles). Distinctly different relative
25 abundances of individual particle types were observed during five characteristic atmospheric
26 situations, namely (a) a mild haze event influenced by local emissions and air mass stagnation,
27 (b) a typical haze event affected by northwestern air masses with a high proportion of sulfate-
28 containing particles, (c) a haze event with a combined influence of northwestern air masses and
29 local emissions, (d) a clean period with low particulate matter concentrations and a blocking
30 pattern, and (e) an event with an enhanced level of heavy metal-containing particles, with Zn,
31 Mn, Ba, Cu, and Pb being the major species identified. Zn-containing particles were mostly
32 released from local sources such as vehicle exhausts and waste incinerations, while Mn, Ba,
33 and Cu-containing particles were attributed to metal-alloy plants or mining. The results suggest



34 that the morphology and chemical compositions of atmospheric aerosol particles in urban area
35 vary depending on their size, sources, and reaction or ageing status, and are affected by both
36 local emissions and long-range air masses.

37

38 Key Words: KORUS-AQ Campaign; low-Z particle EPMA; urban megacity; haze

39

40 **Introduction**

41 Atmospheric aerosols, originating from various anthropogenic and natural sources,
42 have significant impacts on climate change and human health (IPCC, 2021). Anthropogenic
43 emissions greatly influence the composition and behavior of airborne particulate matter (PM)
44 (Kim et al., 2018b; Chowdhury et al., 2018; Nault et al., 2018). On the Korean Peninsula,
45 anthropogenic pollutants primarily come from local emissions and long-range transport air
46 masses (Cho et al., 2021; Park et al., 2020; Choi et al., 2021; Kumar et al., 2021; Nault et
47 al., 2018). Studies have observed changes in the characteristics of aerosols composed of
48 organic and inorganic compounds influenced by different air mass flows. Secondary organic
49 aerosols (SOAs) are particularly affected by local emissions, while inorganic particles can be
50 influenced by either local emissions or long-range transported pollutants (Nault et al., 2018;
51 Kim et al., 2018b; Kim et al., 2020; Park et al., 2018; Chen et al., 2017). Local emissions,
52 including biomass burning, cooking, and traffic exhaust, primarily influence the formation of
53 SOAs in urban areas (Nault et al., 2018; Park et al., 2018; Kim et al., 2018b). On the other
54 hand, transboundary transport of pollutants is significantly affected by comprehensive climatic
55 conditions and can lead to air pollution episodes dominated by inorganic components,
56 including sulfate, nitrate, and ammonium (Kumar et al., 2021; Lee et al., 2019a; Choi et al.,
57 2019).

58 East Asia has seen a significant decline in air quality over the past few decades due to
59 increased emissions of gaseous and particulate pollutants as a result of rapid industrial and
60 economic growth. The Korean Peninsula, surrounded by China, Japan, and Russia, exhibits
61 complex aerosol characteristics influenced by a combination of local emissions, surrounding
62 seas, and transboundary long-range transported air masses (Pochanart et al., 2004; Crawford
63 et al., 2020; Peterson et al., 2019; Ramachandran et al., 2020; Kim et al., 2018a). To further
64 investigate factors affecting air pollution on the Korean Peninsula, an international cooperative
65 field study, the KORUS-AQ (Korea-US Air Quality) campaign, was conducted during May-
66 June 2016 (Crawford et al., 2020). Through this campaign, the temporal and spatial
67 characteristics of various gaseous and particulate pollutants on the Korean Peninsula were



68 successfully elucidated, making it an important study in the field of atmospheric science
69 (**Crawford et al., 2020**). In the Korean Peninsula, ammonium was found to be the most
70 sensitive factor affecting PM_{2.5} exposure, followed by NO_x, SO₂, organic carbon (OC), and
71 black carbon (BC) (**Choi et al., 2019**). The presence of anthropogenic ammonium on the
72 Korean Peninsula leads to the formation of ammonium sulfate (AS) and ammonium nitrate
73 (AN) particles (**Kim et al., 2021; Kim et al., 2020**). Regarding the composition of atmospheric
74 PM₁ in Seoul, the most populated metropolitan area in Korea, OC content was found to be the
75 highest, followed by sulfate, nitrate, ammonium, and BC (**Kim et al., 2018b**).

76 While previous studies have effectively examined the impact of anthropogenic
77 emissions on the formation of submicron particles during the KORUS-AQ campaign, research
78 on supermicron particles remains limited. Aerosol particles in the supermicron fraction, which
79 mainly originate from natural sources like mineral dust and sea-spray aerosols (SSAs), make
80 up a significant proportion of the total aerosol mass (**Andreae and Rosenfeld, 2008; Seinfeld
81 and Pandis, 2006**). Airborne mineral dust particles in East Asia, directly emitted from arid
82 regions of Mongolia and northern China, can undergo physicochemical changes during long-
83 range transportation, for example, through atmospheric reactions with anthropogenic NO_x and
84 SO₂, resulting in the formation of nitrates and sulfates. This leads to alterations in chemical
85 compositions, morphology, size, and radiative forcing capabilities (**Sullivan et al., 2007; Yu
86 et al., 2020; Geng et al., 2014; Heim et al., 2020; Sobanska et al., 2012**). The investigation
87 of the characteristics of supermicron particles, including their particle-particle variability,
88 formation dynamics, and atmospheric fate, is important to gain a comprehensive understanding
89 of the behavior and impact of atmospheric aerosols of natural and anthropogenic origin on air
90 quality and climate change.

91 This study utilized a quantitative electron probe X-ray microanalysis (EPMA)
92 technique based on scanning electron microscopy coupled with X-ray spectrometry, so-called
93 low-Z particle EPMA, to examine the physicochemical characteristics of individual aerosol
94 particles collected at Olympic Park in Seoul, Korea during the KORUS-AQ campaign. Low-Z
95 particle EPMA is a powerful single-particle analytical technique for providing information on
96 unique features of individual aerosol particles, including morphology, elemental compositions,
97 and particle-particle variability (**Geng et al., 2009; Geng et al., 2011; Li et al., 2017; Wu et
98 al., 2019**). Differences in these features are attributed to particle sources, formation
99 mechanisms, and atmospheric fate (**Wu et al., 2019; Song et al., 2022**). This article consists
100 of two parts: (1) an examination of the differences in physicochemical characteristics based on
101 particle species and (2) an analysis of the temporal variations of individual aerosol particles



102 during the KORUS-AQ campaign. The characterization of individual particles, combined with
103 other studies on atmospheric aerosols during the KORUS-AQ period, provides valuable
104 insights into the unique features of urban atmospheric particles.

105

106 **2. Experiments**

107 **2.1 Sampling**

108 Ambient aerosol particles were collected at Olympic Park (37.52° N, 127.12° E) in
109 Seoul, the capital of South Korea (Fig. S1 in Supporting Information). The Seoul metropolitan
110 area (SMA), with high population density, numerous local emissions, and transboundary long-
111 range transport, provides a suitable location for investigating the complex characteristics of
112 atmospheric aerosols (Kim et al., 2018b; Kim et al., 2020). A 3-stage cascade Dekati PM10
113 impactor (Dekati Ltd.) with an aerodynamic cut-off size of 10, 2.5, and 1.0 μm for stages 1-3
114 at a 10 L min^{-1} flow rate, respectively, was used to collect aerosol particles on Al foils. Each
115 sample set was analyzed for particles collected on stages 2 and 3, corresponding to $\text{PM}_{2.5-10}$
116 and $\text{PM}_{1-2.5}$, respectively. A total of 52 sets of samples were collected in the morning and
117 evening (9:00 ~ 10:00 and 15:00 ~ 16:00, KST) during May 23 to June 5, 2016. The sampling
118 duration for each stage was controlled to obtain an optimum number of particles without
119 overloading on the Al foils. 72-hour backward air mass trajectories were generated using the
120 HYSPLIT (Hybrid Single-Particle Lagrangian Integrated Trajectory) model for different
121 receptor heights of 250 m, 500 m, and 1000 m above ground level. The HYSPLIT model is
122 available at the NOAA Air Resources Laboratory's website
123 (<http://www.arl.noaa.gov/ready/hysplit4.html>).

124

125 **2.2 Determination of individual particle types by low-Z particle EPMA**

126 The physicochemical characteristics of individual aerosol particles were examined
127 using a SEM (JEOL JSM-6390) equipped with an Oxford Link SATW ultrathin window EDX
128 detector. The resolution of the detector was 133 eV for Mn-K α X-rays, and X-ray spectra were
129 recorded using INCA Oxford software (Oxford Instruments Analytical Ltd, INCA suite version
130 4.09). Routine measurement was conducted using an accelerating voltage of 10 kV and beam
131 current of 0.5 nA, while 20 kV and 0.25 nA were used to confirm heavy metal elements of
132 specific particles. To obtain sufficient X-ray counts for quantitative analysis, a typical
133 measurement time of 15 s was chosen. The net X-ray intensities for the elements were obtained



134 using a non-linear least-squares fitting of the collected spectra using the AXIL program
135 (Vekemans et al., 1994). The elemental concentrations of the individual particles were
136 determined from their X-ray intensities using a Monte Carlo calculation combined with reverse
137 successive approximations (Ro et al., 2001, 2002). The chemical species of individual aerosol
138 particles were determined based on their size, morphology, and elemental composition.

139

140 **3 Results and discussion**

141 **3.1 Characteristics and abundances of individual particle types**

142 Individual particles were classified into 13 species based on their morphology and
143 elemental composition, and further categorized into seven major groups based on their sources
144 and/or formation mechanism. These groups are (1) secondary aerosol particles including SOAs
145 and secondary organic and inorganic aerosols (SOIAs), (2) genuine and aged/reacted mineral
146 dust, (3) reacted SSAs, (4) combustion particles, (5) Fe-rich particles, (6) heavy metal-
147 containing particles, and (7) others, including biogenic and humic-like substances (HULIS)
148 particles. More information on the classification can be found in the Supporting Information
149 (Section A and Tables S1).

150

151 *3.1.1 Secondary aerosol particles (SOAs and SOIAs)*

152 Secondary aerosol particles, including SOAs and SOIAs, account for 5.6% and 29.3%
153 in the PM_{2.5-10} and PM_{1-2.5} fractions, respectively. These particles, likely formed through gas-
154 to-particle conversion, photochemical processes, and the condensation of semi-volatile organic
155 compounds (Hallquist et al., 2009; Kim et al., 2018a), are significantly more abundant in the
156 fine PM_{1-2.5} fraction than in the PM_{2.5-10} fraction. The morphology, X-ray spectra, and elemental
157 compositions of typical secondary aerosol particles are presented in Fig. 1. SOA particles
158 appear as dark droplets in their secondary electron image (SEI) and are primarily composed of
159 C and O (>90% in low-Z particle EPMA analysis) (Fig. 1a). The spread droplet-like
160 morphology of SOA particles collected on the hydrophilic Al foil suggests that they are likely
161 low-viscous and water-soluble. In contrast, SOIAs, which are mixtures of SOA and inorganic
162 constituents such as NH₄⁺, NO₃⁻, and/or SO₄²⁻, exhibit C, N, O, and S in their X-ray spectra and
163 are apparently susceptible to damage by electron beams (Figs. 1b and 1c). The morphology of
164 SOIA particles varies depending on the organic and inorganic contents. Those with high
165 inorganic content appear as bright, crystalline shapes surrounded by a water-soluble footprint
166 (Fig. 1b), while those with a high organic content resemble dark droplets (Fig. 1c). An inset

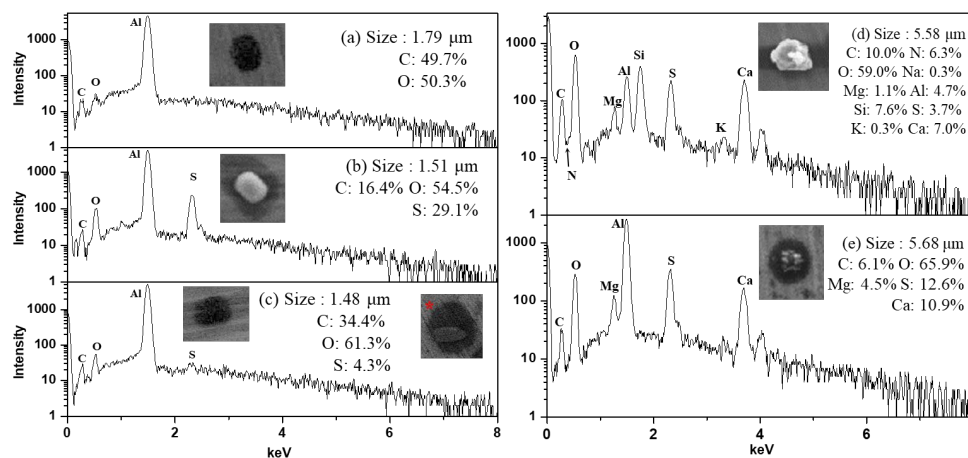


Figure 1. Morphology, X-ray spectra, and elemental compositions of (a) SOA, (b) SOIA (high inorganic), (c) SOIA (high organic), (d) reacted aluminosilicate, and (e) reacted carbonate particles.

167

168 marked with * on Fig. 1c shows a SOIA particle that appears as a core-shell structure, with a
169 SOIA core surrounded by a dark droplet shade mainly containing C and O. The differences in
170 the crystalline morphology of SOIAs indicate that the heterogeneous nucleation and/or
171 crystallization of particles can vary depending on the chemical species present (Wu et al.,
172 2020). Furthermore, the significant water-soluble footprint surrounding SOA and SOIA
173 particles indicates that aqueous-phase chemistry is a crucial process in the formation of
174 secondary aerosol particles in the urban area of Seoul. Previous studies have reported that SOA
175 particles in South Korea are primarily influenced by local emissions, while the sources of
176 inorganic components are highly relevant to both local emissions and transboundary long-range
177 transport air masses (Nault et al., 2018; Kim et al., 2018b; Choi et al., 2019).

178

179 3.1.2 Mineral dust particles

180 Genuine and reacted mineral dust particles are the most abundant particle types among
181 the seven major ones in this study, accounting for 73.2% and 44.5% in the PM_{2.5-10} and PM_{1-2.5}
182 fractions, respectively. These mineral dust particles are irregularly shaped and appear bright
183 in SEI, mainly consisting of crustal elements such as Al, Si, Ca, Mg, K, and others. The
184 observed chemical species of mineral dust particles include aluminosilicates (such as feldspar,
185 muscovite, montmorillonite, illite, kaolinite, talc, pyrophyllite, etc.), quartz (SiO₂), carbonates
186 (calcite (CaCO₃), dolomite (CaMg(CO₃)₂), and magnesite (MgCO₃)), TiO₂, and their
187 reacted/aged ones. Genuine mineral dust particles, tending to be larger in size, are significantly



188 more abundant in the $PM_{2.5-10}$ fraction than in the $PM_{1-2.5}$ fraction, whereas the proportion of
 189 reacted minerals is slightly higher in the $PM_{1-2.5}$ fraction (71.0%) compared to the $PM_{2.5-10}$
 190 (66.2%) due to the larger specific surface area of $PM_{1-2.5}$ particles, making them more prone to
 191 chemical reactions in the air.

192 The reactivity of mineral dust particles varies depending on their chemical species and
 193 size, as shown in Table 1. In the $PM_{2.5-10}$ fractions, particles are highly associated with nitrate
 194 compared to sulfate (46.2% vs. 30.0%), while the abundance of sulfate is comparatively higher
 195 than nitrate for $PM_{1-2.5}$ particles (34.3% vs. 20.0%), indicating that sulfate formation occurs
 196 more frequently in smaller particles. The proportion of reacted particles is significantly higher
 197 in carbonate particles than in aluminosilicates (93.9% vs. 56.2%), indicating that carbonate
 198 mineral dust has a higher reactivity than aluminosilicates. Reacted aluminosilicate particles
 199 appear bright and irregular, being surrounded by water-soluble moieties (Fig. 1d), implying
 200 that the chemical reaction mostly occurred on the surface, while reacted carbonate species show
 201 dark lumpy, core-shell shapes (Fig. 1e), indicating that the reaction readily occurred from the
 202 surface to the internal part. Further analysis reveals that the carbonate particles tend to react
 203 with sulfate, while aluminosilicates were more likely to interact with nitrate (Table 1). The
 204 different abundances of sulfate and nitrate in the reacted mineral particles not only depend on
 205 the particle species and size, but also on the source, transport pathway, and formation process
 206 (Geng et al., 2011, 2014; Sullivan et al., 2007). These findings suggest that (a) carbonate
 207 minerals are more sensitive to changes in atmospheric conditions than aluminosilicates, and (b)
 208 carbonate minerals react with sulfate before nitrate due to the prevailing neutralization by
 209 sulfate (Takahashi et al., 2014; Matsuki et al., 2005; Seinfeld and Pandis., 2006; Sullivan
 210 et al., 2017).

211

Table 1. Relative abundances of genuine and reacted mineral dust and SSA particles

Type	Genuine	Reacted			% of reacted particles	
		Containing-N	Containing-S	Containing-both		
$PM_{2.5-10}$						
Mineral dust	Aluminosilicates	23.2%	17.9%	4.9%	5.8%	55.2%
	Carbonates	1.5%	8.5%	6.9%	4.5%	92.9%
Sea spray aerosols			4.5%	2.9%	5.1%	100%
$PM_{1-2.5}$						
Mineral dust	Aluminosilicates	12.1%	5.0%	7.7%	3.4%	57.2%
	Carbonates	0.8%	3.6%	10.2%	1.6%	95.0%
Sea spray aerosols			4.4%	9.4%	2.0%	100%

212



213

214 3.1.3 Sea-spray aerosols (SSAs)

215 Nascent SSAs are rich in characteristic elements such as Na, Mg, and Cl, as indicated
216 by their X-ray spectra. They are released into the atmosphere from the sea surface through film
217 drops and jet drops caused by bubble bursting (**Eom et al., 2016; Cochran et al., 2017**).
218 Freshly emitted SSAs are a mixture of inorganic Na, Mg, and Cl and organic compounds such
219 as fatty acids, amino acids, and liposaccharides, which are closely related to the biological
220 activity of micro-organisms in the marine environment (**Eom et al., 2016; Cochran et al.,**
221 **2017**). Once released into the atmosphere, these nascent SSAs tend to react with various acidic
222 species such as sulfuric, nitric, and organic acids to form reacted/aged SSAs. All SSAs for both
223 PM_{2.5-10} and PM_{1-2.5} fractions were found to be in the reacted form (Table 1), despite their short
224 transport distances (~50–100 km until they reach the sampling site from the Yellow Sea),
225 suggesting that they are susceptible to atmospheric reactions (**Laskin et al., 2003; Gupta et**
226 **al., 2015; Li et al., 2017; Chen et al., 2020**). As shown in Table 1, the reacted SSAs accounted
227 for 12.4% and 15.7% in the PM_{2.5-10} and PM_{1-2.5} fractions, respectively, in which the nitrate-
228 containing SSAs were more abundant than the sulfate-containing ones in the PM_{2.5-10} fraction
229 (9.6% vs. 8.4%), while those containing sulfates were more abundant in the PM_{1-2.5} fraction
230 (11.3 vs. 6.4%), indicating that sulfate formation occurs more in smaller SSA particles. The
231 higher abundance of SSAs containing both nitrates and sulfates in the larger size fraction may
232 be attributed to the availability of sufficient anions to accumulate acidic cations, which is
233 associated with a decrease in acidity as particle size increases (**Angle et al., 2021**).

234

235 3.1.4 Combustion particles

236 The combustion particles include soot agglomerates, tar balls, fly ash, and char particles,
237 accounting for 1.3% and 2.8% in the PM_{2.5-10} and PM_{1-2.5} fractions, respectively. Most
238 elemental carbon (EC) particles, such as soot agglomerates, tar balls, and char particles, have
239 similar elemental compositions, but they can be differentiated based on their unique
240 morphology (Fig. 2 and Table S1).

241 Soot agglomerates are remnants of incomplete combustion and are formed through the
242 vaporization-condensation mechanism (**Bond et al., 2004; Chen et al., 2006**). Based on their
243 morphology and elemental compositions, soot agglomerates can be classified into two types:
244 fresh and aged. The fresh soot agglomerates appear bright and have a characteristic chain-like
245 structure with fractal geometry, as shown in the right-side SEI of Fig. 2a. The complex
246 geometry of the soot agglomerates provides an active area for the deposition of gaseous or



247 particulate species. The morphology of aged soot agglomerates shown in Fig. 2a is more
248 compact than that of the fresh ones. The aging of the soot agglomerates is attributed to several
249 mechanisms such as oxidation, absorption or condensation of gaseous species, and coagulation
250 with other particles. This aging process can cause the soot agglomerates to shrink and
251 restructure into a more compact shape, as shown in Fig. 2a (Bond et al, 2004; Zhang et al.,
252 2008; Chen et al., 2006).

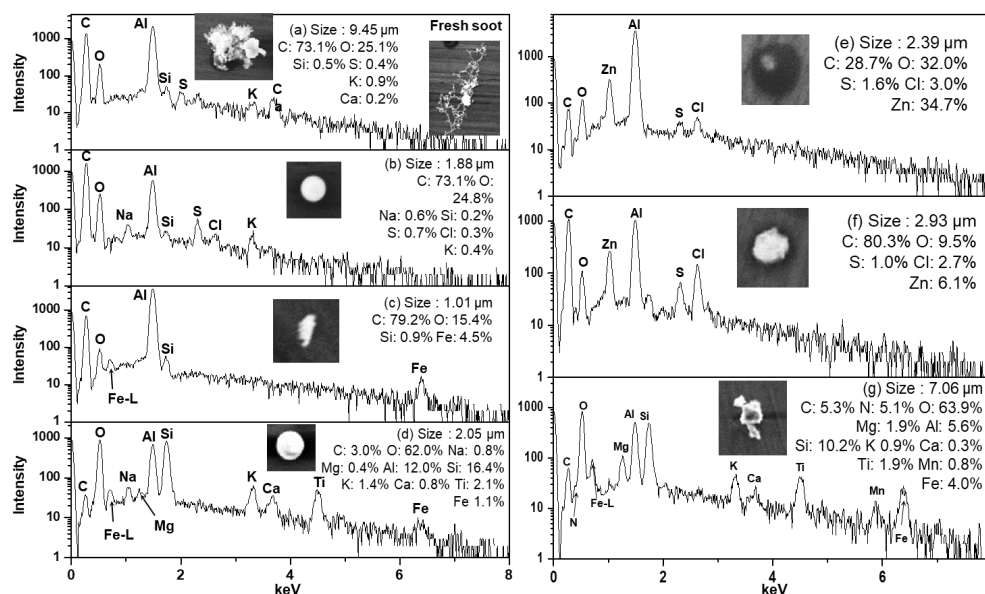


Figure 2. Morphology, X-ray spectra, and elemental compositions of (a) aged soot aggregates, (b) tar balls, (c) char, (d) fly ash, (e) and (f) Zn-HMs, and (g) Mn/Ti-HMs.

253 Tar ball particles are composed of organic oligomers and are a representative particle
254 type from smoldering combustions such as biomass burning or biofuel combustion (Adachi et
255 al., 2019; Giroto et al., 2018; Pósfai et al., 2004). The spherical shape of the tar ball particles
256 (Fig. 2b) results from post-physical and chemical transformation of the organic matter. The
257 formation of the tar balls can vary depending on factors such as oligomerization of organics,
258 condensation, photochemical processes, water loss, and temperature changes, leading to
259 different internal structures (Tóth et al., 2018; Adachi et al., 2019).

260 Char particles are incomplete combustion residues of liquid or solid carbonaceous fuel
261 materials, appearing compact and irregular in shape on the SEI, as shown in Fig. 2c (Chen et
262 al., 2006).



263 Fly ash particles, as shown in Fig. 2d, have a similar elemental composition to
264 aluminosilicate mineral particles but with a distinct bright spherical shape on the SEI. These
265 particles were rarely found in both size fractions, accounting for 0.08% and 0.42% in PM_{2.5-10}
266 and PM_{1-2.5} fractions, respectively. The spherical morphology of fly ash particles is attributed
267 to their formation mechanism, which involves rapid cooling after being released from high-
268 temperature combustion at industrial plants (Geng et al., 2011).

269

270 3.1.5 Heavy metal-containing particles (HMs)

271 Particles containing heavy metal elements (HMs), such as Zn, Pb, Cu, Mn, Ba, Zr, Sr,
272 Cd, As, Cr, V, Ni, Sn, and Co, are of particular concern due to their adverse impact on human
273 health. In this study, a significant number of HMs were observed, accounting for 2.7% and 4.4%
274 in the PM_{2.5-10} and PM_{1-2.5} fractions, respectively. Among the 14 types of HMs observed, Zn,
275 Pb, Ba, Cu, and Mn were frequently encountered (Fig. 3). HMs can be released from both
276 anthropogenic and natural sources, with thermal power plants, vehicle exhaust, battery
277 manufacture, and the metallurgical industry being some of the most common anthropogenic
278 sources (Tian et al., 2015; Xu et al., 2004). Tracing the sources of HMs during the KORUS-
279 AQ campaign can be done based on coexisting elements, morphologies, and relative
280 abundances.

281

282

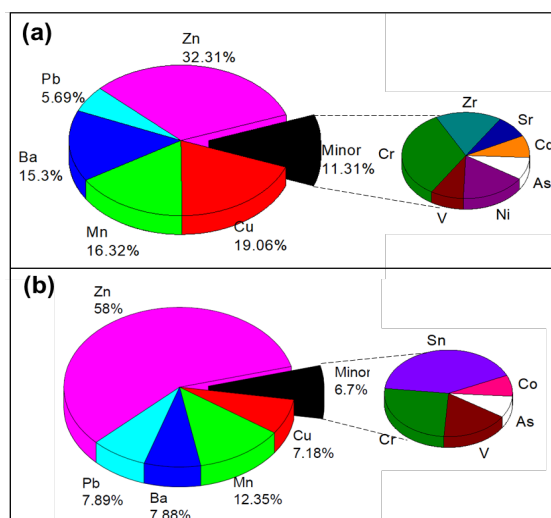


Figure 3. Heavy metals observed in HMs for (a) PM_{2.5-10} and (b) PM_{1-2.5} fractions.



283 As shown in Fig. 3, the most abundant type of HMs observed in this study were Zn-
284 containing particles (Zn-HMs), accounting for 32.3% and 58.0% of the total HMs in PM_{2.5-10}
285 and PM_{1-2.5}, respectively. Zn-HMs can be emitted from various anthropogenic sources such as
286 waste incineration, vehicle emissions, rubber tire wear, and coal combustion (**Hopke et al.,**
287 **1991; Chow et al., 2004; Hjortenkrans et al., 2007**). In the sampling site, which is an urban
288 area with heavy traffic, Zn-HMs may be attributed to vehicle emissions such as rubber tire and
289 brake pad wear. Two major identified types of Zn-HMs were C-Zn-Cl and C-Zn-Cl + (N or S)
290 (Fig. 2e and 2f), which made up 54.4% and 29.8% of the total Zn-HMs, respectively. A
291 significant proportion (84.9%) of Zn-HMs were observed to contain Cl, likely due to
292 incomplete atmospheric reactions of ZnCl₂. ZnCl₂ can easily undergo aqueous-phase chemical
293 reactions in the atmosphere due to its hygroscopic nature. The presence of N or S on the X-ray
294 spectra and dark droplet morphology on the SEI of the Zn-HMs indicate that the particles had
295 undergone atmospheric reactions with NO_x/SO_x (**Moffet et al., 2008**). The temporal variations
296 of Zn-HMs will be discussed in Section 3.2.

297 A total of 20 Pb-HMs were observed in this study, in the forms of mixtures with SSAs
298 (8 particles), Pb-Cl-other heavy metals (6 particles), mineral dust (4 particles), and Pb-As (2
299 particles). They were likely emitted from vehicle exhaust and coal-fired power plants (**Lee et**
300 **al., 2019b**). Among the 39 Mn-HMs observed, 24 particles were associated with mineral dust,
301 coexisting mainly with Al, Si, Ca, and Mg; 6 particles with Fe; 2 particles with SSAs; 4
302 particles with Mg, Cl, and S; and 3 particles with F. They might originate from natural soil or
303 anthropogenic sources such as ore-crushing plants, ferroalloy plants, and similar facilities
304 (**Moreno et al., 2011**). The morphology and elemental composition of a Mn-HM are shown in
305 Fig. 2g. Among the total 33 Cu-HMs, 17 particles were mixed with Fe, followed by the mineral
306 dust form (10 particles), and minor forms such as Cu-C-S and Cu-C-N-O (6 particles). Major
307 sources of atmospheric Cu include non-ferrous metal plants, mining, and smelting complexes
308 (**Choi et al., 2013; Eichler et al., 2014**). Among the total of 30 Ba-HMs, 17 particles were
309 mixed with Fe, followed by mineral dust (5 particles), BaSO₄ (3 particles), and other minor
310 forms (5 particles). Ba-HMs could be released from natural sources in the form of barite
311 (BaSO₄) and witherite (BaCO₃), and anthropogenic sources such as ore crushing plants, mining,
312 refining, and manufacture of barium products (**Choudhury et al., 2009; Beddows et al., 2004**).
313 The fact that Mn, Ba, and Cu-HMs appear abundantly as a mixture of Fe or mineral dust
314 suggests that their major source might be ferroalloy plants, mining, or ore crushing plants.

315

316 *3.1.6 Fe-rich, biogenic, and HULIS particles*



317 Fe-rich particles, which have an irregular shape and appear bright on the SEI, usually
318 contain more than 20% Fe in elemental concentration. These particles account for 1.7% and
319 2.2% in the $PM_{2.5-10}$ and $PM_{1-2.5}$ fractions, respectively, and likely originate from steel
320 production, metallurgical industries, and the abrasion of brake linings (Geng et al., 2011).

321 Biogenic particles, primarily originating from natural sources (Martin et al., 2010), are
322 relatively more abundant in the $PM_{2.5-10}$ fraction (2.83%) than the $PM_{1-2.5}$ fraction (0.81%).
323 They can be identified by their unique morphologies and the presence of minor elements such
324 as Na, Mg, N, K, P, S, and/or Cl (Ro et al., 2002; Geng et al., 2011). In this study, most of the
325 observed biogenic particles were attributed to trichomes, plant fragments, pollen, or spores, as
326 their sizes were generally larger than 2 μm (Matthias-Maser et al., 2000; Coz et al., 2010).
327 Typical examples of biogenic particles are displayed in Fig. S2a-c, corresponding to fungal
328 spores, micro-organism, and trichomes or leaf fragments, respectively.

329 The HULIS particles, consisting mainly of water-insoluble organic carbon (WISOC),
330 are characterized by high C and O content and unique morphology. There are 17 out of 8004
331 particles, only accounting for 0.2%. They might be released from soil, wetland, and sewage-
332 treatment plants.

333
334

335 **3.2 Temporal chemical composition variations of individual aerosol particles during the** 336 **KORUS-AQ campaign**

337 Based on differences in relative abundances of individual particle types, ambient PM
338 concentrations (Fig. S3), and backward air mass trajectories (Fig. S4), the sampling period
339 (5/23–6/5) of the KORUS-AQ campaign was divided into five characteristic atmospheric
340 situations as follows: (Period I, 5/23) - a SOA dominant period influenced by local emissions
341 and air mass stagnation; (Period II, 5/25-5/28) - a SOIA-rich haze episode with the influence
342 of long-range transported air-masses; (Period III, 5/29-5/31) - haze events with the combined
343 influence of long-range transported air-masses and local emissions; (Period IV, 6/1-6/3) - a
344 clean air period; and (Period V, 6/4-6/5) - a period dominantly influenced by local emissions.
345 The relative abundances of individual particle types are shown in Fig. 4. There are significant
346 differences over the sampling period, especially in the $PM_{1-2.5}$ fractions.

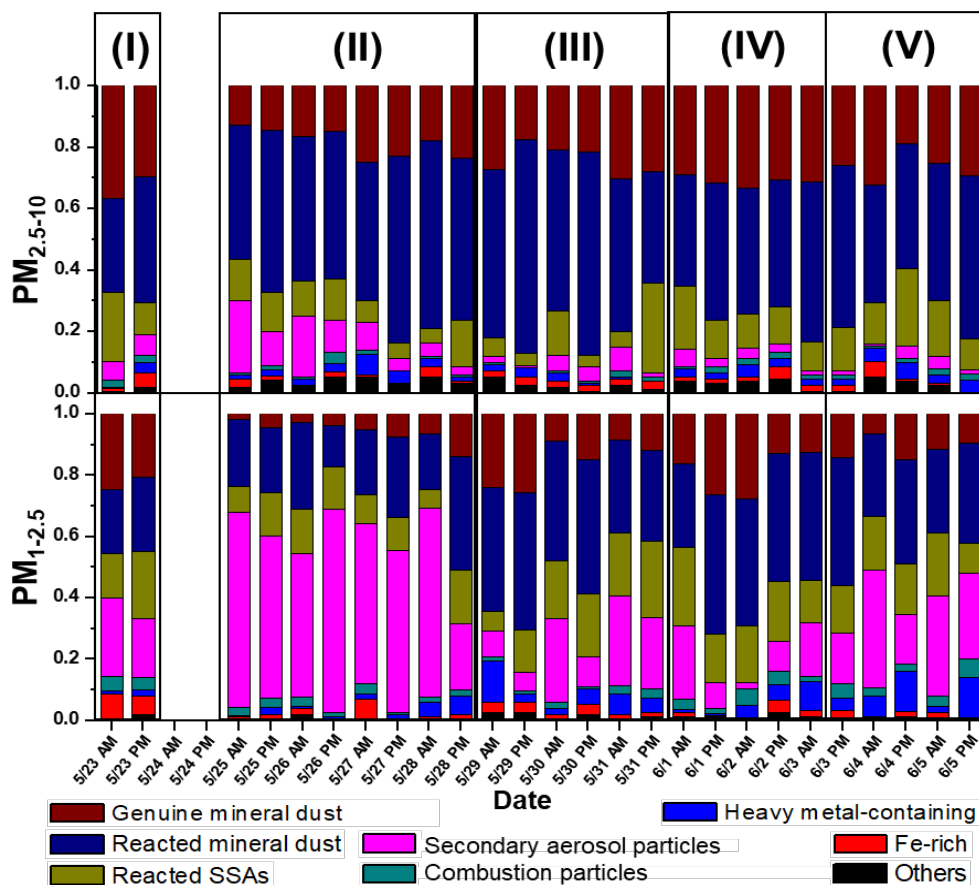


Figure 4. Relative abundances of various particle types in the PM_{2.5-10} and PM_{1-2.5} fractions.

347

348 **Period I (5/23)**

349 On 5/23, the first day of the sampling period, individual aerosol particles showed clear
 350 distinctions in morphology and elemental compositions, particularly for secondary aerosol
 351 particles. As shown in Fig. 5a, most secondary aerosol particles in the PM_{1-2.5} fraction,
 352 including SOA and SOIA, had dark droplet morphology, indicating that their major chemical
 353 species are organic carbon. Figure 6 highlights a significant increase in the ratio of SOA to
 354 secondary aerosol particles. The SOA/secondary aerosol particles ratio of the PM_{1-2.5} fraction
 355 was notably higher (55.2%) in the 5/23 sample compared to the average for the overall samples
 356 during the campaign (22.0%), emphasizing the enhanced contribution of organic carbon to
 357 secondary aerosol particle formation. Figure 7 shows that the proportion of combustion



358 particles increased by 1.8 and 1.6 times compared to the overall average in the PM_{2.5-10} and
359 PM_{1-2.5} fractions, respectively. A slightly elevated PM concentration on 5/23 (Fig. S3) suggests
360 mild air pollution on that day. Our findings align with other bulk studies that confirmed an
361 increased proportion of organic carbon in PM₁ aerosols during 5/17-5/23 (Kim et al., 2018a;
362 Kim et al., 2018b). Stagnant conditions under a persistent anticyclone prevented the transport
363 of pollutants from other regions, suggesting a dominant influence of local emissions during
364 this period (Kim et al., 2018b; Peterson et al., 2019; Heim et al., 2020). The formation of
365 SOA in South Korea, particularly in urban areas, was reported to be predominantly influenced
366 by local emissions (Nault et al., 2018). Consequently, the rise in the proportion of organic
367 carbon during Period I can be attributed to the augmented contribution of local emissions to
368 the formation of secondary aerosol particles due to air mass stagnation (Peterson et al., 2019;
369 Kim et al., 2018a; Kim et al., 2018b; Crawford et al., 2021). The enhanced level of
370 combustion particles also suggests the contribution of local emissions. Overall, the data from
371 5/23 indicate a clear influence of local emissions on aerosol particle composition and
372 concentration.

373

374 Period II (5/25-5/28)

375 After the rainfall on 5/24, the morphology, elemental composition, and relative
376 abundance of individual aerosol particles during 5/25-5/28 (Period II) differed significantly
377 compared to those observed in Period I. In terms of particle morphology, Fig. 5b shows that
378 SOIA particles on 5/25 exhibited a bright crystalline morphology, suggesting that these
379 particles are primarily composed of inorganic components such as sulfate, nitrate, and

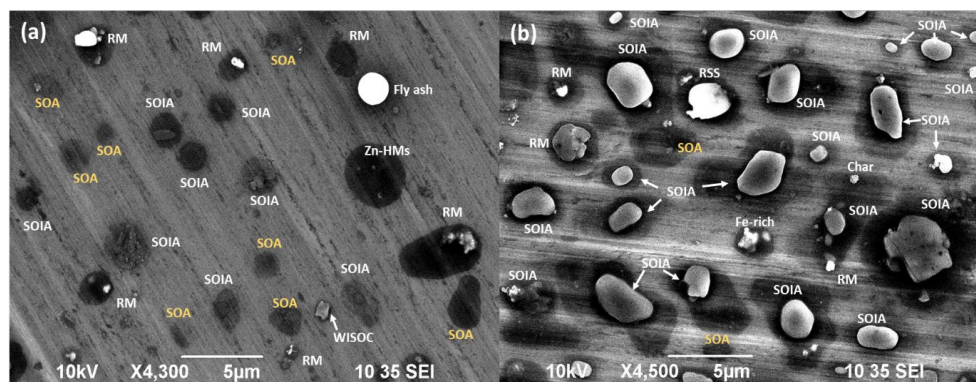


Figure 5. Typical secondary electron images of PM_{1-2.5} aerosol particles collected on (a) 5/23 PM and (b) 5/25 AM. (RM : reacted mineral dust)



380 abundance of individual aerosol particles during 5/25-5/28 (Period II) differed significantly
381 compared to those observed in Period I. In terms of particle morphology, Fig. 5b shows that
382 SOIA particles on 5/25 exhibited a bright crystalline morphology, suggesting that these
383 particles are primarily composed of inorganic components such as sulfate, nitrate, and
384 ammonium, as described in Section 3.2.1. These bright crystalline SOIA particles mostly
385 contain high sulfur contents, as shown in Fig. 1b, suggesting that their major composition is
386 likely ammonium sulfate (AS) (Wu et al., 2019). Ammonium-rich conditions in East Asia
387 facilitate the existence of secondary particles in AS or AN forms (Kim et al., 2020; Kim et al.,
388 2021). The ratio of SOIA particles to total particles increased dramatically during Period II, as
389 shown in Fig. 6. In the $PM_{1-2.5}$ fraction, the proportion of SOIA particles out of the total
390 particles increased significantly to 61.5% on 5/25, compared to the overall average of 24%,
391 and remained high at 46.3% during Period II. Additionally, the reacted/aged mineral dust and
392 SSA particles containing sulfate were dominant during Period II both in the $PM_{1-2.5}$ and $PM_{2.5-10}$
393 fractions. The drastic increase in ambient PM concentration during this period (Figure S3) is
394 indicative of an air pollution (haze) episode. In contrast to Period I, which is considered to be
395 influenced mainly by local emissions due to air mass stagnation, the drastic increase in sulfate
396 composition of secondary aerosols, reacted mineral dust, and reacted SSA particles during

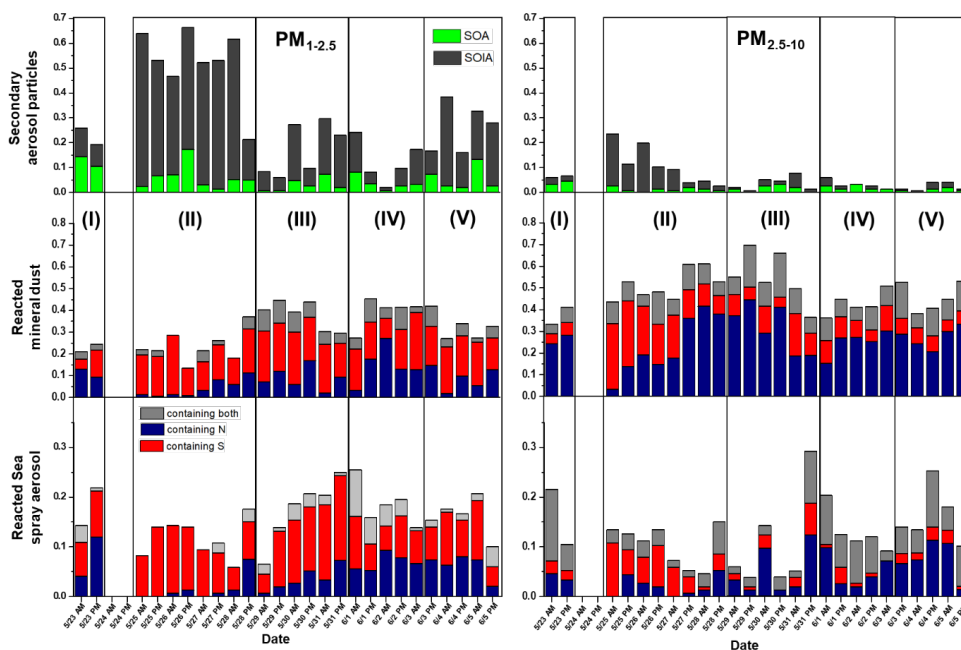


Figure 6. Relative abundances of secondary aerosols, reacted mineral dust, and reacted SSA particles during the KORUS-AQ campaign.



397 Period II seems to be driven by other external factors than local emissions. As shown in Fig.
398 S4b, air mass transportation from northeastern China at low altitudes (250 m A.G.L) was
399 observed during this haze episode, which contrasts with Period I. Mild southwesterly winds
400 (<5 m/s) facilitate the transport of pollutants from China to the study region (**Peterson et al.,**
401 **2019; Nault et al., 2018; Heim et al., 2020; Choi et al., 2019**). An elevated level of secondary
402 inorganic constituents, including sulfate, nitrate, and ammonium, was also reported during this
403 period (**Kim et al., 2018a; Kim et al., 2018b; Song et al., 2022**). The humid conditions (RH
404 > 60%) sustained during this period provided a favorable environment for the formation of
405 secondary particles (SIA and SOA) (**Peterson et al., 2019**). Also, sulfate-containing mineral
406 dust and SSA particles were abundantly observed because the air masses were buffered rapidly
407 with sulfate when they passed through urban and industrial areas during long-range
408 transportation (**Yu et al., 2020**). Overall, the data from Period II suggest a significant influence
409 of long-range transported air masses from northeastern China on the composition and
410 concentration of aerosol particles in the study region.

411

412 **Period III (5/29-5/31)**

413 The relative abundances of individual particles during 5/29-5/31 (Period III) differed
414 from those of 5/25-5/28 (Period II), despite consistently high PM concentrations during the
415 period (Fig. S3) and air mass flow from Northeastern China (Figs. S4c and S4d). During Period
416 III, the proportion of SOIA particles decreased to 14.4% compared to 46.3% in Period II (Fig.
417 6). Concurrently, the proportions of reacted mineral dust and SSA particles increased with a
418 noticeable increase in nitrate-containing ones (Fig. 6). The increase in nitrate-containing
419 particles in the urban area suggests a strong influence of local emissions (**Yan et al., 2015**).
420 Changes in the relative abundances of individual HM particles were also noticeable (Fig. 7).
421 The proportion of Zn-HMs increased rapidly from 0.8% during Period II to 2.8% during Period
422 III, suggesting an elevated influence of local emissions, given that the major sources of Zn-
423 HMs are local emissions (section 3.1.5). The proportion of other HMs also somewhat increased
424 to 2.8% compared to the overall average of 1.9%. The changes in the relative abundances of
425 individual particles observed in this study are fairly different from other bulk studies in which
426 air pollution episodes with consistently high inorganic contents were observed during 5/25-
427 5/31 (**Kim et al., 2018a; Kim et al., 2018b**). Similar to Period II, weak westerly winds
428 facilitated the transport of pollutants during Period III; however, the formation of secondary
429 particles appears to be relatively reduced due to ~20% lower RH compared to Period II
430 (**Peterson et al., 2019**). Additionally, as shown in Figs. S4b and S4c, during Period III, the



431 travel distance and residence time within the Korean Peninsula were longer relative to Period
432 II, suggesting an increased mixing of transported and local pollutants. Based on the decrease
433 in the proportion of secondary aerosol particles formed mainly through gas-particle conversion
434 and the increase in the reacted forms of the primary aerosol particles, including mineral dust
435 and SSAs, it is plausible that aggregation or mixing between individual particles intensified
436 during Period III. Overall, the changes in particle abundances during Period III indicate a
437 complex interplay of local emissions and long-range transport. The decrease in secondary
438 aerosol particles and the increase in reacted primary aerosol particles, along with the elevated
439 proportions of Zn-HMs and other HMs, suggest intensified mixing of pollutants from various
440 sources during this period.
441

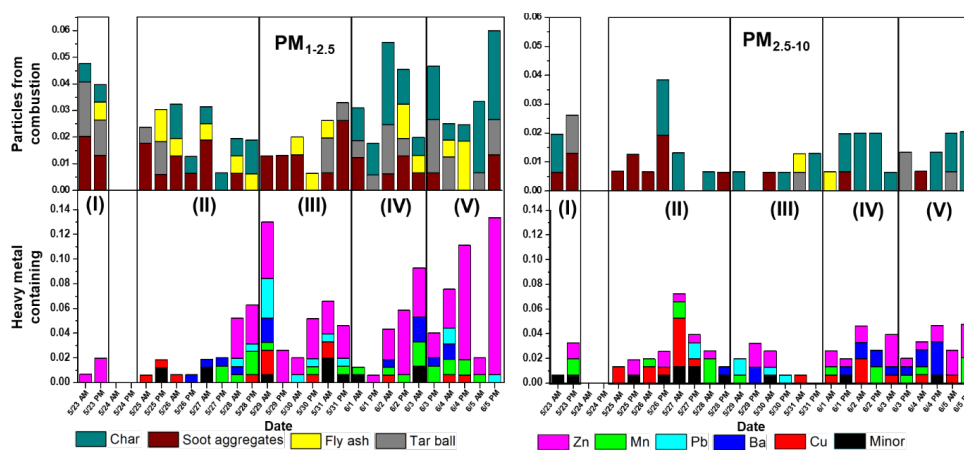


Figure 7. Relative abundances of combustion particles and heavy metal-containing particles during the KORUS-AQ campaign.

442 **Period IV (6/1-6/3)**

443 After a series of air pollution episodes, ambient PM concentrations decreased
444 drastically from 6/1 (Fig. S3). The relative abundance of individual particle types during 6/1-
445 6/3 manifested distinct differences compared to Periods I-III. During Period IV, the proportion
446 of secondary aerosol particles decreased to 12.9%, compared to an overall average of 29.2%,
447 while the proportion of genuine mineral dust particles increased from an overall average of
448 12.9% to 18.3% (Fig. 4). An increase in nitrate-containing reacted mineral dust and SSA
449 particles was observed in both size fractions (Fig. 6). Zn-HMs from local emissions were also
450 frequently encountered during this period (Fig. 7). Moreover, an increase in tar balls and char
451 particles was observed (Fig. 7). Increases in nitrate-containing particles, Zn-HMs, and



452 combustion particles suggest an intensified influence of local emissions. Additionally, it was
453 reported that a blocking pattern influenced by high atmospheric pressure was observed over
454 East Asia during this period, which minimized the transportation of pollutants from other Asian
455 mainland areas (Heim et al., 2020; Peterson et al., 2019). This blocking pattern could have
456 contributed to the increased influence of local emissions and the observed rise in nitrate-
457 containing particles, Zn-HMs, and combustion particles during Period IV. Overall, the data
458 from Period IV suggest that local emissions played a dominant role in shaping the aerosol
459 composition during this period, with limited influence from long-range transported air masses.
460 The decrease in secondary aerosol particles and the increase in genuine mineral dust particles
461 and locally emitted pollutants such as Zn-HMs and combustion particles further support this
462 conclusion.

463

464 **Period V (6/4-6/5)**

465 Ambient PM concentrations slightly increased during Period V compared to Period
466 IV (Fig. S3). There was a noticeable increase in Zn-HMs during this period, with the proportion
467 of Zn-HM increasing from an average of 2.6% to 6.6%. This increase was particularly
468 noticeable during the afternoon hours (Fig. 7) and might be related to heightened weekend
469 traffic, as the sampling area is a park surrounded by thoroughfares (Fig. S1). In addition, the
470 proportion of secondary aerosol particles increased drastically to 28.8% compared to 12.9% in
471 Period IV, and the proportion of combustion particles somewhat increased to 3.6% compared
472 to an average of 2.6%. Air mass trajectories shown in Fig. S4f suggest an intensified influence
473 from inland Korea during Period V, resulting in the increased levels of particles from local
474 emissions and secondary aerosol particles. When the air mass travels a short distance (~250
475 km/day), urban areas could be primarily influenced by local emissions (Lee et al., 2019a).
476 Continued blocking patterns from Period IV effectively exclude pollutant transport from
477 outside areas, but occasionally lead to stagnant conditions (Peterson et al., 2019). Overall, the
478 changes in particle abundances during Period V indicate an intensified influence of local
479 emissions and secondary aerosol particles, likely due to weekend traffic and stagnant
480 conditions. The increase in Zn-HMs and combustion particles further supports the impact of
481 local anthropogenic emissions on air quality during this period. Efforts to manage and control
482 local emission sources, including vehicle emissions, waste incineration, and fossil fuel
483 combustions, could play a crucial role in improving air quality in the urban area.

484

485 **4. Conclusions**



486 Individual aerosol particles collected at Olympic Park, Seoul, Korea, during the
487 KORUS-AQ campaign were analyzed using low-Z particle EPMA. A total of 8004 particles
488 from 52 samples were examined to identify their chemical species, particle-particle variability,
489 sources, and atmospheric fate. The major constituents in the $PM_{2.5-10}$ and $PM_{1-2.5}$ fractions were
490 mineral dust, SSAs, and secondary aerosol particles. However, the relative abundance of
491 individual particle types varied depending on changes in air mass flow and differences in
492 emission sources. The reacted mineral dust and reacted SSA particles containing nitrate were
493 abundant in the $PM_{2.5-10}$ fraction, whereas sulfate-containing ones were relatively higher in the
494 $PM_{1-2.5}$ fraction. Of particular interest, heavy metals were found to account for a relatively high
495 proportion of particles both in the $PM_{2.5-10}$ (2.65%) and $PM_{1-2.5}$ (4.42%) fractions, with Zn, Pb,
496 Ba, Mn, and Cu being the major species. Zn and Pb are mainly released from sources such as
497 waste incineration, vehicle exhaust, and coal-fired power plants, while Mn, Ba, and Cu are
498 primarily released from mining and metal alloy industries.

499 The relative abundances of secondary aerosol particles varied significantly during the
500 sampling period, reflecting changes in air mass stagnation and emission sources. During the
501 haze episodes, sulfate-containing particles, including SOIA, mineral dust, and SSAs, were
502 predominant, and the proportion of SOA particles increased as local influence intensified.
503 During the clean period of 6/1-6/3, nitrate-containing particles were abundantly observed,
504 indicating a high contribution of NO_x emissions from local sources. Zn-HMs from local sources
505 such as vehicle emissions and waste incineration were noticeably observed during 6/4-6/5
506 when the air mass stagnated over the Korean peninsula.

507 The temporal variations in the abundance and physicochemical characteristics of
508 individual aerosol particles provide valuable insights into the behavior and emission sources
509 of atmospheric urban aerosols. The changes in the composition of organic and inorganic
510 components resulted in distinct morphological and crystalline structures of secondary aerosol
511 particles, influencing properties such as hygroscopic behavior and radiative forcing. The
512 relative abundance of HMs, particularly those containing Zn, effectively reveals the impact of
513 local emissions such as vehicle emissions and waste incineration. The highly hygroscopic
514 nature of the observed Zn-HMs suggests a potential threat to human health, as they are prone
515 to adsorbing or reacting with other organic and inorganic components in the atmosphere. The
516 observed changes in the abundance of particles from typical combustion events and secondary
517 aerosol particles emphasize the need to manage local emission sources to maintain air quality.
518 The complexity of aerosol particle behavior highlights the importance of a comprehensive



519 understanding of the interplay between local emissions, long-range transport, and
520 meteorological conditions to develop effective air pollution mitigation strategies.

521

522 **Code and data availability**

523 The data set is available upon request from Chul-Un Ro (curo@inha.ac.kr).

524

525 **Author contributions**

526 **Chul-Un Ro (RCU)** and **Geng Hong (GH)** designed and supervised the entire experimental
527 program, provided guidance on the quantitative analysis of individual particles, and reviewed
528 the manuscript. **Hanjin Yoo (HJY)** conducted the single-particle analysis, analyzed the data,
529 and wrote the manuscript. **Li Wu (LW)** reviewed the manuscript and provided feedback on
530 the manuscript. All authors read and approved the final manuscript.

531

532 **Competing interests**

533 The authors declare that they have no conflict of interest.

534

535 **Financial Support**

536 This study was supported by the National Research Foundation of Korea (NRF) grant funded
537 by the Korean government (MSIT) (No. 2021R1A4A1032579 and No. 2021R1A2C2004240)
538 and by the National Institute of Environmental Research (NIER) funded by the Ministry of
539 Environment (MOE) of Korea (NIER-2021-03-03-007). The authors thank for a fund from the
540 China State High-end Foreign Expert Recruitment Project (G2022004013L).

541

542 **Supporting Information**

543 Table S1 and Figures S1-S4

544

545 **References**

546

- 547 Adachi, K., Sedlacek, A. J., Kleinman, L., Springston, S. R., Wang, J., Chand, D., Hunne, J.
548 M., Shilling, J. E., Onasch, T. B., Kinase, T., Sakata, K., Takahashi, Y., and Buseck, P.
549 R.: Spherical tarball particles from through rapid chemical and physical changes of
550 organic matter in biomass-burning smoke, *Proc. Natl. Acad. Sci. U.S.A.*, 116, 19336-
551 19341, www.pnas.org/cgi/doi/10.1073/pnas.1900129116, 2019.
- 552 Andreae, M. O., and Rosenfeld, D.: Aerosol-cloud-precipitation interactions. Part 1. The nature
553 and sources of cloud-active aerosols, *Earth Sci. Rev.*, 89, 13-41,
554 doi:10.1016/j.earscirev.2008.03.001, 2008.
- 555 Angle, K. J., Crocker, D. R., Simpson, R. M. C., Mayer, K. J., Garofalo, L. A., Moore, A. N.,
556 Garcia, S. L. M., Or, V. W., Srinivasan, S., Farhan, M., Sauer, J. S., Lee, C., Pothier,



- 557 M. A., Farmer, D. K., Martz, T. R., Bertram, T. H., Cappa, C. D., Prather, K. A., and
558 Grassian, V. H.: Acidity across the interface from the ocean surface to sea spray aerosol,
559 Proc. Natl. Acad. Sci. U.S.A., 118(2), e2018397118,
560 <https://doi.org/10.1073/pnas.2018397118>, 2021.
- 561 Beddows, D. C. S., Donovan, R. J., Harrison, R. M., Heal, M. R., Kinnersley, R. P., King, M.
562 D., Nicholson, D. H., and Thompson, K. C.: Correlations in the chemical composition
563 of rural background atmospheric aerosol in UK determined in real time using time-of-
564 flight mass spectrometry, J. Environ. Monit., 6, 124-133,
565 <https://doi.org/10.1039/B311209H>, 2004.
- 566 Bond, T. C., Streets, D. G., Yarber, K. F., Nelsom, S. M., Woo, J.-H., and Klimont, Z.: A
567 technology-based global inventory of black and organic carbon emissions from
568 combustion, J. Geophys. Res., 109, D14203, doi:10.1029/2003JD003697, 2004.
- 569 Chen, L., Peng, C., Gu, W., Fu, H., Jian, X., Zhang, H., Zhang, G., Zhu, J., Wang, X., and Tang,
570 M.: On mineral dust aerosol hygroscopicity, Atmos. Chem. Phys., 20, 13611–13626,
571 <https://doi.org/10.5194/acp-20-13611-2020>, 2020.
- 572 Chen, S., Huang, J., Kang, L., Wang, H., Ma, X., He, Y., Yuan, T., Yang, B., Huang, Z., and
573 Zhang, G.: Emission, transport, and radiative effects of mineral dust from the
574 Taklimakan and Gobi deserts: Comparison of measurements and model results, Atmos.
575 Chem. Phys., 17, 2401–2421, <https://doi.org/10.5194/acp-17-2401-2017>, 2017.
- 576 Chen, Y., Shah, N., Huggins, F. E., and Huffman, G. P.: Microanalysis of ambient particles
577 from Lexington, KY, by electron microscopy, Atmos. Environ., 40, 651-663,
578 doi:10.1016/j.atmosenv.2005.09.036, 2006.
- 579 Cho, C., Schwarz, J. P., Perring, A. E., Lamb, K. D., Kondo, Y., Park, J. U., Park, D. H., Shim,
580 K., Park, J. S., Park, R. J., Lee, M., Song, C. K., and Kim, S. W.: Light-absorption
581 enhancement of black carbon in the Asian outflow inferred from airborne SP2 and in-
582 situ measurements during KORUS-AQ, Sci. Tot. Environ., 773,
583 <https://doi.org/10.1016/j.scitotenv.2021.145531>, 2021.
- 584 Choi, J. kyu, Heo, J. B., Ban, S. J., Yi, S. M., and Zoh, K. D.: Source apportionment of PM_{2.5}
585 at the coastal area in Korea, Sci. Tot. Environ., 447, 370–380,
586 <https://doi.org/10.1016/j.scitotenv.2012.12.047>, 2013.
- 587 Choi, J., Park, R. J., Lee, H.-M., Lee, S., Jo, D. S., Jeong, J. I., Henze, D. K., Woo, J.-H., Ban,
588 S.-J., and Lee, M.-D.: Impacts of local vs. trans-boundary emissions from different
589 sectors on PM_{2.5} exposure in South Korea during the KORUS-AQ campaign, Atmos.
590 Environ., 203, 196-205, 10.1016/j.atmosenv.2019.02.008, 2019.
- 591 Choi, Y., Ghim, Y. S., Rozenhaimer, M. S., Redemann, J., LeBlanc, S. E., Flynn, C. J., Johnson,
592 R. J., Lee, Y., Lee, T., Park, T., Schwarz, J. P., Lamb, K. D., and Perring, A. E.:
593 Temporal and spatial variations of aerosol optical properties over the Korean Peninsula
594 during KORUS-AQ, Atmos. Environ., 254, 118301,
595 <https://doi.org/10.1016/j.atmosenv.2021.118301>, 2021.
- 596 Choudhury, H., Carey, R.: Barium and barium compounds, Concise Int. Chem. Assessment
597 Doc. 33. Int. Progr. Chem. Safety, World Health Organ., Geneva, 2009.
- 598 Chow, J. C., Watson, J. G., Kuhns, H., Etyemezian, V., Lowenthal, D. H., Crow, D., Kohl, S.
599 D., Engelbrecht, J. P., and Green, M. C.: Source profiles for industrial, mobile, and area
600 sources in the Big Bend Regional Aerosol Visibility and Observational study,
601 Chemosphere, 54, 185-208, 10.1016/j.chemosphere.2003.07.004, 2004.
- 602 Chowdhury, P. H., He, Q., Male, T. L., Brune, W. H., Rudich, Y., and Pardo, M.: Exposure of
603 lung epithelial cells to photochemically aged secondary organic aerosol shows increased
604 toxic effects, Environ. Sci. Technol. Lett., 5, 424-430, doi:10.1021/acs.estlett.8b00256,
605 2018.



- 606 Cochran, R. E., Laskina, O., Trueblood, J. V., Estillore, A. D., Morris, H. S., Jayarathne, T.,
607 Sultana, C. M., Lee, C., Lin, P., Laskin, J., Laskin, A., Dowling, J. A., Qin, Z., Cappa,
608 C. D., Bertram, T. H., Tivanski, A. V., Stone, E. A., Prather, K. A., and Grassian, V.
609 H.: Molecular diversity of sea spray aerosol particles: impact of ocean biology on
610 particle composition and hygroscopicity, *Chem*, 2(5), 655-667,
611 <https://doi.org/10.1016/j.chempr.2017.03.007>, 2017.
- 612 Coz, E., Artíñano, B., Clark, L. M., Hernandez, M., Robinson, A. L., Casuccio, G. S., Lersch,
613 T. L., and Pandis, S. N.: Characterization of fine primary biogenic organic aerosol in
614 an urban area in the northeastern United States, *Atmos. Environ.*, 44(32), 3952-3962,
615 <https://doi.org/10.1016/j.atmosenv.2010.07.007>, 2010.
- 616 Crawford, J. H., Ahn, J.-Y., Al-Saadi, J., Change, L., Emmons, L. K., Kim, J., Lee, G., Park,
617 J.-H., Park, R. J., Woo, J. H., Song, C.-K., Hong, J.-H., Hong, Y.-D., Lefer, B. L., Lee,
618 M., Lee, T., Kim, S., Min, K.-E., Yum, S.-Y., Shin, H. J., Kim, Y.-W., Choi, J.-S., Park,
619 J.-S., Szykman, J. J., Long, R. W., Jordan, C. E., Simpson, I. J., Fried, A., Dibb, J. E.,
620 Cho, S. Y., Kim, Y. P.: The Korea–United States Air Quality (KORUS-AQ) field study,
621 *Elementa*. 9., 00163, <https://doi.org/10.1525/elementa.2020.00163>, 2021.
- 622 Eichler, A., Tobler, L., Eyrikh, S., Malygina, N., Papina, T., and Margit, S.: Ice-core based
623 assessment of historical anthropogenic heavy metal (Cd, Cu, Sb, Zn) emissions in the
624 Soviet Union, *Environ. Sci. Technol.*, 48, 2635-2642, [dx.doi.org/10.1021/es404861n](https://doi.org/10.1021/es404861n),
625 2014.
- 626 Eom, H. J., Gupta, D., Cho, H. R., Hwang, H. J., Hur, S. D., Gim, Y., and Ro, C. U.: Single-
627 particle investigation of summertime and wintertime Antarctic sea spray aerosols using
628 low-Z particle EPMA, Raman microspectrometry, and ATR-FTIR imaging techniques,
629 *Atmos. Chem. Phys.*, 16, 13823–13836, <https://doi.org/10.5194/acp-16-13823-2016>,
630 2016.
- 631 Geng, H., Jung, H.-J., Park, Y., Hwang, H., Kim, H., Kim, Y. J., Sunwoo, Y., and Ro, C.-U.:
632 Morphological and chemical composition characteristics of summertime atmospheric
633 particles collected at Tokchok Island, Korea, *Atmos. Environ.*, 43, 3364-3373,
634 [10.1016/j.atmosenv.2009.03.034](https://doi.org/10.1016/j.atmosenv.2009.03.034), 2009.
- 635 Geng, H., Ryu, J., Maskey, S., Jung, H.-J., and Ro, C.-U.: Characterization of individual
636 aerosol particles collected during a haze episode in Incheon, Korea using the
637 quantitative ED-EPMA technique, *Atmos. Chem. Phys.*, 10, 26641-26676,
638 [10.5194/acp-11-1327-2011](https://doi.org/10.5194/acp-11-1327-2011), 2011.
- 639 Geng, H., Hwang, H., Liu, X., Dong, S., and Ro, C.-U.: Investigation of aged aerosols in size-
640 resolved Asian dust storm particles transported from Beijing, China, to Incheon, Korea,
641 using low-Z particle EPMA, *Atmos. Chem. Phys.*, 14, 3307, [10.5194/acp-14-3307-](https://doi.org/10.5194/acp-14-3307-2014)
642 2014, 2014.
- 643 Giroto, G., China, S., Bhandari, J., Gorkowski, K., Scarnato, B. v., Capek, T., Marinoni, A.,
644 Veghte, D. P., Kulkarni, G., Aiken, A. C., Dubey, M., and Mazzoleni, C.: Fractal-like
645 Tar Ball Aggregates from Wildfire Smoke, *Environ. Sci. Technol. Lett.*, 5, 360–365,
646 <https://doi.org/10.1021/acs.estlett.8b00229>, 2018.
- 647 Gupta, D., Eom, H.-J., Cho, H.-R., and Ro, C.-U.: Hygroscopic behavior of NaCl–MgCl₂
648 mixture particles as nascent sea-spray aerosol surrogates and observation of
649 efflorescence during humidification, *Atmos. Chem. Phys.*, 15, 11273-11290,
650 <https://doi.org/10.5194/acp-15-11273-2015>, 2015.
- 651 Hallquist, M., Wenger, J. C., Baltensperger, U., Rudich, Y., Simpson, D., Claeys, M., Dommen,
652 J., Donahue, N. M., George, C., Goldstein, A. H., Hamilton, J. F., Herrmann, H.,
653 Hoffmann, T., Iinuma, Y., Jang, M., Jenkin, M. E., Jimenez, J. L., Kiendler-Scharr, A.,
654 Maenhaut, W., McFiggans, G., Mentel, Th. F., Monod, A., Prévôt, A. S. H., Seinfeld,
655 J. H., Surratt, J. D., Szmigielski, R., and Wildt, J.: The formation, properties and impact



- 656 of secondary organic aerosol: current and emerging issues, *Atmos. Chem. Phys.*, 9,
657 5155–5236, <https://doi.org/10.5194/acp-9-5155-2009>, 2009.
- 658 Heim, E. W., Dibb, J., Scheuer, E., Jost, P. C., Nault, B. A., Jimenez, J. L., Peterson, D., Knote,
659 C., Fenn, M., Hair, J., Beyersdorf, A. J., Corr, C., and Anderson, B. E.: Asian dust
660 observed during KORUS-AQ facilitates the uptake and incorporation of soluble
661 pollutants during transport to South Korea, *Atmos. Environ.*, 224,
662 <https://doi.org/10.1016/j.atmosenv.2020.117305>, 2020.
- 663 Hjortenkrans, D. S., Bergbäck, B. G., and Häggerud, A. V.: Metal emissions from brake linings
664 and tires: case studies of Stockholm, Sweden 1995/1998 and 2005, *Environ. Sci.
665 Technol.*, 41, 5224-5230, 10.1021/es070198o, 2007.
- 666 Hopke, P. K.: An introduction to receptor modeling, *Chemometrics and Intelligent Laboratory
667 Systems*, 10, 21-43, 10.1016/0169-7439(91)80032-L, 1991.
- 668 IPCC, 2021: Climate Change 2021: The Physical Science Basis. Contribution of Working
669 Group I to the Sixth Assessment Report of the Intergovernmental Panel on Climate
670 Change [Masson-Delmotte, V., P. Zhai, A. Pirani, S.L. Connors, C. Péan, S. Berger, N.
671 Caud, Y. Chen, L. Goldfarb, M.I. Gomis, M. Huang, K. Leitzell, E. Lonnoy, J.B.R.
672 Matthews, T.K. Maycock, T. Waterfield, O. Yelekçi, R. Yu, and B. Zhou (eds.)].
673 Cambridge University Press. In Press.
- 674 Kim, E., Kim, B.-U., Kim, H. C., and Kim, S.: Direct cross impacts of upwind emission control
675 on downwind PM_{2.5} under various NH₃ conditions in Northeast Asia, *Environ. Pollut.*,
676 268, 115794, <https://doi.org/10.1016/j.envpol.2020.115794>, 2021.
- 677 Kim, N., Park, M., Yum, S. S., Park, J. S., Shin, H. J., and Ahn, J. Y.: Impact of urban aerosol
678 properties on cloud condensation nuclei (CCN) activity during the KORUS-AQ field
679 campaign, *Atmos. Environ.*, 185, 221-236, 0.1016/j.atmosenv.2018.05.019, 2018a.
- 680 Kim, N., Yum, S. S., Park, M., Park, J. S., Shin, H. J., and Ahn, J. Y.: Hygroscopicity of urban
681 aerosols and its link to size-resolved chemical composition during spring and summer
682 in Seoul, Korea, *Atmos. Chem. Phys.*, 20, 11245–11262, [https://doi.org/10.5194/acp-
683 20-11245-2020](https://doi.org/10.5194/acp-20-11245-2020), 2020.
- 684 Kim, H., Zhang, Q., and Heo, J.: Influence of intense secondary aerosol formation and long-
685 range transport on aerosol chemistry and properties in the Seoul Metropolitan Area
686 during spring time: results from KORUS-AQ, *Atmos. Chem. Phys.*, 18, 7149-7168,
687 <https://doi.org/10.5194/acp-18-7149-2018>, 2018b.
- 688 Kumar, N., Park, R. J., Jeong, J. I., Woo, J.-H., Kim, Y., Johnson, J., Yarwood, G., Kang, S.,
689 Chun, S., and Knipping, E.: Contributions of international sources to PM_{2.5} in South
690 Korea, *Atmos. Environ.*, 261, 118542, <https://doi.org/10.1016/j.atmosenv.2021.118542>,
691 2021.
- 692 Laskin, A., Gaspar, D. J., Wang, W., Hunt, S. W., Cowin, J. P., Colson, S. D., and Finlayson-
693 Pitts, B. J.: Reactions at interfaces as a source of sulfate formation in sea-salt particles,
694 *Science*, 301(5631), 340-344, DOI:10.1126/science.1085374, 2003.
- 695 Lee, S., Kim, J., Choi, M., Hong, J., Lim, H., Eck, T. F., Holben, B. N., Ahn, J. Y., Kim, J.,
696 and Koo, J. H.: Analysis of long-range transboundary transport (LRTT) effect on
697 Korean aerosol pollution during the KORUS-AQ campaign, *Atmos. Environ.*, 204, 53–
698 67, <https://doi.org/10.1016/j.atmosenv.2019.02.020>, 2019a.
- 699 Lee, S., Shin, D., Han, C., Choi, K.-S., Hur, S. D., Lee, J., Byun, D.-S., Kim, Y.-T., and Hong,
700 S.: Characteristic concentrations and isotopic composition of airborne lead at urban,
701 rural and remote sites in western Korea, *Environ. Pollut.*, 254, 113050,
702 <https://doi.org/10.1016/j.envpol.2019.113050>, 2019b.
- 703 Li, X., Gupta, D., Lee, J., Park, G., and Ro, C.-U.: Real-time investigations of chemical
704 compositions and hygroscopic properties of aerosols generated from NaCl and Malonic



- 705 acid solutions using in situ Raman microspectrometry, *Environ. Sci. Technol.*, 51(1),
706 263-270, <https://doi.org/10.1021/acs.est.6b04356>, 2017.
- 707 Martin, S. T., Andreae, M. O., Artaxo, P., Baumgardner, D., Chen, Q., Goldstein, A. H.,
708 Guenther, A., Heald, C. L., Mayol-Bracero, O. L., McMurry, P. H., Pauliquevis, T.,
709 Pöschl, U., Prather, K. A., Roberts, G. C., Saleska, S. R., Silva Dias, M. A., Spracklen,
710 D. V., Swietlicki, E., and Trebs, I.: Sources and properties of Amazonian aerosol
711 particles, *Rev. Geophys.*, 48, RG2002, [10.1029/2008rg000280](https://doi.org/10.1029/2008rg000280), 2010.
- 712 Matsuki, A., Iwasaka, U., Shi, G., Zhang, D., Trochkin, D., Yamada, M., Kim, Y.-S., Chen,
713 B., Nagatani, T., Miyazawa, T., Nagatani, M., and Nakata, H.: Morphological and
714 chemical modification of mineral dust: Observational insight into the heterogeneous
715 uptake of acidic gases, *Geophys. Res. Lett.*, 32, 1-4, doi:10.1029/2005GL024176, 2005.
- 716 Matthias-Maser, S., Obolkin, V., Khodzer, T., and Jaenicke, R.: Seasonal variation of primary
717 biological aerosol particles in the remote continental region of Lake Baikal/Siberia,
718 *Atmos. Environ.*, 34, 3805-3811, doi.org/10.1016/S1352-2310(00)00139-4, 2000.
- 719 Moffet, R. C., Desyaterik, Y., Hopkins, R. J., Tivanski, A. V., Gilles, M. K., Wang, Y.,
720 Shutthanandan, V., Molina, L. T., Abraham, R. G., and Johnson, K. S.: Characterization
721 of aerosols containing Zn, Pb, and Cl from an industrial region of Mexico City, *Environ.*
722 *Sci. Technol.*, 42, 7091-7097, [10.1021/es7030483](https://doi.org/10.1021/es7030483), 2008.
- 723 Moreno, T., Pandolfi, M., Querol, X., Lavín, J., Alastuey, A., Viana, M., and Gibbons, W.:
724 Manganese in the urban atmosphere: identifying anomalous concentrations and sources,
725 *Environ. Sci. Pollut. Res.*, 18, 173-183, DOI 10.1007/s11356-010-0353-8, 2011.
- 726 Nault, B. A., Campuzano-Jost, P., Day, D. A., Schroder, J. C., Anderson, B., Beyersdorf, A. J.,
727 Blake, D. R., Brune, W. H., Choi, Y., Corr, C. A., de Gouw, J. A., Dibb, J., Digangi, J.
728 P., Diskin, G. S., Fried, A., Gregory Huey, L., Kim, M. J., Knute, C. J., Lamb, K. D.,
729 Lee, T., Park, T., Pusede, S. E., Scheuer, E., Thornhill, K. L., Woo, J. H., and Jimenez,
730 J. L.: Secondary organic aerosol production from local emissions dominates the organic
731 aerosol budget over Seoul, South Korea, during KORUS-AQ, *Atmos. Chem. Phys.*, 18,
732 17769–17800, <https://doi.org/10.5194/acp-18-17769-2018>, 2018.
- 733 Park, M., Yum, S. S., Kim, N., Anderson, B. E., Beyersdorf, A., Thornhill, K. L.: On the
734 submicron aerosol distributions and CCN activity in and around the Korean Peninsula
735 measured onboard the NASA DC-8 research aircraft during the KORUS-AQ field
736 campaign, *Atmos. Res.*, 243, 105004, <https://doi.org/10.1016/j.atmosres.2020.105004>,
737 2020.
- 738 Park, S., Yu, G. H., and Lee, S.: Optical absorption characteristics of brown carbon aerosols
739 during the KORUS-AQ campaign at an urban site, *Atmos. Res.*, 203, 16–27,
740 <https://doi.org/10.1016/j.atmosres.2017.12.002>, 2018.
- 741 Peterson, D. A., Hyer, E. J., Han, S.-O., Crawford, J. H., Park, R. J., Holz, R., Kuehn, R. E.,
742 Eloranta, E., Knot, C., Jordan, C. E., and Lefer, B. L.: Meteorology influencing
743 springtime air quality, pollution transport, and visibility in Korea, *Elementa*. 9., 7, 57,
744 <https://doi.org/10.1525/elementa.395>, 2019.
- 745 Pochanart, P., Wild, O., and Akimoto, H. (2004). Air pollution import to and export from East
746 Asia. In: Stohl, A. (eds) *Air Pollution. The Handbook of Environmental Chemistry*, vol
747 4G. Springer, Berlin, Heidelberg. <https://doi.org/10.1007/b94525>
- 748 Pósfai, M., Gelencsér, A., Simonics, R., Arató, K., Li, J., Hobbs, P. v., and Buseck, P. R.:
749 Atmospheric tar balls: Particles from biomass and biofuel burning, *J. Geophys. Res.*
750 *Atmos.*, 109, <https://doi.org/10.1029/2003jd004169>, 2004.
- 751 Ramachandran, S., Rupakheti, M., and Lawrence, M. G.: Aerosol-induced atmospheric heating
752 rate decreases over South and East Asia as a result of changing content and composition.
753 *Sci. Rep.*, 10, 20091, doi.org/10.1038/s41598-020-76936-z, 2020.



- 754 Ro, C.-U., Oh, K.-Y., Kim, H., Kim, H., Kim, H., Kim, Y. P., Lee, C. B., Kim, K.-H., Kang,
755 C. H., and Osán, J.: Single-particle analysis of aerosols at Cheju Island, Korea, using
756 low-Z electron probe X-ray microanalysis: A direct proof of nitrate formation from sea
757 salts, *Environ. Sci. Technol.*, 35, 4487-4494, 10.1021/es0155231, 2001.
- 758 Ro, C.-U., Kim, H., Oh, K.-Y., Yea, S. K., Lee, C. B., Jang, M., and Van Grieken, R.: Single-
759 particle characterization of urban aerosol particles collected in three Korean cities using
760 low-Z electron probe X-ray microanalysis, *Environ. Sci. Technol.*, 36, 4770-4776,
761 10.1021/es025697y, 2002.
- 762 Seinfeld, J. H., and Pandis, S. N.: *Atmospheric chemistry and physics: from air pollution to*
763 *climate changes*. 2nd edition, John Wiley & Sons, New York, 2006.
- 764 Sobanska, S., Hwang, H., Choël, M., Jung, H. J., Eom, H. J., Kim, H., Barbillat, J., and Ro, C.
765 U.: Investigation of the chemical mixing state of individual Asian dust particles by the
766 combined use of electron probe X-ray microanalysis and Raman microspectrometry,
767 *Anal. Chem.*, 84, 3145-3154, <https://doi.org/10.1021/ac2029584>, 2012.
- 768 Song, M., Park, J., Lim, Y., Oh, S.-H., Lee, J. Y., Lee, K.-H., Ro, C.-U., and Bae, M.-S.: Long-
769 range transport impacts from biomass burning and secondary pollutant sources based
770 on receptor models during KORUS-AQ campaign, *Atmos. Environ.*, 276, 119060,
771 <https://doi.org/10.1016/j.atmosenv.2022.119060>, 2022.
- 772 Sullivan, R. C., Guazzotti, S. A., Sodeman, D. A., and Prather, K. A.: Direct observations of
773 the atmospheric processing of Asian mineral dust, *Atmos. Chem. Phys.*, 7, 1213-1236,
774 <https://doi.org/10.5194/acp-7-1213-2007>, 2007.
- 775 Takahashi, Y., Higashi, N., Furukawa, T., Miyoshi, T., Fujiwara, M., and Uematsu, M.: A
776 study of the chemical processes in aerosols and their impacts on the environment using
777 X-ray absorption fine structure spectroscopy, *W-PASS.*, 43-50, doi:10.5047/w-
778 pass.a01.005, 2014.
- 779 Tian, H. Z., Zhu, C. Y., Gao, J. J., Cheng, K., Hao, J. M., Wang, K., Hua, S. B., Wang, Y., and
780 Zhou, J. R.: Quantitative assessment of atmospheric emissions of toxic heavy metals
781 from anthropogenic sources in China: historical trend, spatial distribution, uncertainties,
782 and control policies, *Atmos. Chem. Phys.*, 15, 10127-10147, doi:10.5194/acp-15-
783 10127-2015, 2015.
- 784 Tóth, Á., Hoffer, A., Pósfai, M., Ajtai, T., Kónya, Z., Blazsó, M., Czégény, Z., Kiss, G., Bozóki,
785 Z., and Gelesér, A.: Chemical characterization of laboratory-generated tar ball particles,
786 *Atmos. Chem. Phys.*, 18, 10407-10418, doi.org/10.5194/acp-18-10407-2018, 2018.
- 787 Vekeman, B., Janssens, K., Vincze, L., Adams, F., and Epsen, P. V.: Analysis of X-ray spectra
788 by iterative least squares (AXIL): New developments, *X-ray Spectrometry*, 23(6),
789 278-285, 10.1002/xrs.1300230609, 1994.
- 790 Wu, L., Li, X., Kim, H., Geng, H., Godoi, R. H. M., Barbosa, C. G. G., Godoi, A. F. L.,
791 Yamamoto, C. I., de Souza, R. A. F., Pöhlker, C., Andreae, M. O., and Ro, C. U.:
792 Single-particle characterization of aerosols collected at a remote site in the Amazonian
793 rainforest and an urban site in Manaus, Brazil, *Atmos. Chem. Phys.*, 19, 1221-1240,
794 <https://doi.org/10.5194/acp-19-1221-2019>, 2019.
- 795 Wu, L., Becote, C., Sobanska, S., Flaud, P.-M., Perraudin, E., Villenave, E., Song, Y.-C., and
796 Ro, C.-U.: Hygroscopic behavior of aerosols generated from solutions of 3-methyl-
797 1,2,3-butanetricarboxylic acid, its sodium salts, and its mixtures with NaCl, *Atmos.*
798 *Chem. Phys.*, 20, 14103-14122, <https://doi.org/10.5194/acp-20-14103-2020>, 2020.
- 799 Xu, M. H., Yan, R., Zheng, C. G., Qiao, Y., Han, J., and Sheng, C. D.: Status of trace element
800 emission in a coal combustion process: a review, *Fuel Process. Technol.*, 85, 215-223,
801 doi:10.1016/S0378-3820(03)00174-7, 2004.



- 802 Yan, J., Chen, L., Lin, Q., Li, Z., Chen, H., and Zhao, S.: Chemical characteristics of submicron
803 aerosol particles during a long-lasting haze episode in Xiamen, China, *Atmos. Environ.*,
804 113, 118-126, 10.1016/j.atmosenv.2015.05.003, 2015.
- 805 Yu, Z., Zhang, M., Kim, S., Bae, C., Koo, B., Beardsley, R., Park, J., Chang, L. S., Lee, H. C.,
806 Lim, Y.-K., and Cho, J. H.: Simulating the impact of long-range-transported Asian
807 mineral dust on the formation of sulfate and nitrate during the KORUS-AQ Campaign,
808 *ACS Earth Space Chem.*, 4, 1039-1049,
809 <https://dx.doi.org/10.1021/acsearthspacechem.0c00074>, 2020.
- 810 Zhang, R., Khalizov, A. F., Pagels, J., Zhang, D., Xue, H., and McMurry, P. H.: Variability in
811 morphology, hygroscopicity, and optical properties of soot aerosols during atmospheric
812 processing, *Proc. Natl. Acad. Sci. U.S.A.*, 105(30), 10291-10296,
813 doi/10.1073/pnas.0804860105, 2008.